Direct numerical simulation of sound absorption in porous media

Milan Červenka, Michal Bednařík
Czech Technical University in Prague, Faculty of Electrical Engineering, Technická 2, 166 27 Prague 6, Czech Republic.

Tomasz G. Zieliński
Institute of Fundamental Technological Research of the Polish Academy of Sciences, ul. Pawinskiego 5B, 02-106 Warsaw, Poland.

Summary
Numerical simulation of absorption of sound in porous media is an important part of the design of the treatments for the environmental noise reduction. In the porous media, the mechanical energy carried by sound is dissipated by thermo-viscous interactions with the solid surface of the media frame, which usually has complicated geometry at the microscopic (sub-millimetre) scale. In order to be able to absorb the acoustic energy at the low frequencies of interest, a layer of porous material must be rather thick (at the order of centimetres). This is why direct numerical simulation (DNS) of the sound absorption in porous media is a rather computationally challenging task because small geometrical details must be properly resolved in a large computational domain. In order to avoid these difficulties, simplified semi-phenomenological models introducing so called effective fluid have been proposed. For example, the Johnson-Champoux-Allard-Pride-Lafarge (JCAPL) model is based on eight parameters which can be measured or calculated based on the media micro-structural geometry. Within this work, we compare the numerical results obtained by the 3D DNS with the prediction of the JCAPL model in case of several porous media represented by closely-packed spheres. The DNS calculations are performed using the linearised Navier-Stokes equations for layers of spheres of different thicknesses, the parameters for the JCAPL model are calculated subsequently using Laplace, Poisson, and Stokes-flow analyses on a representative volume element of the media. Very good agreement between the results has been found.

PACS no. 43.55.Ev

1. Introduction

We live in a modern world, surrounded by technology. The technology makes our life easy. However, we pay for this technological comfort – we have to deal with an omnipresent noise. Even if there are advanced techniques for the noise reduction, we mostly rely on porous sound-absorbing materials. These materials employ microscopic fibres or pores to convert the acoustic energy, carried with noise, into heat. The compliance with hygienic standards related to exposure to noise is a part of the design process, which is substantially simplified by numerical simulations. Even if the direct numerical simulations (DNS) of the processes taking place in porous media are straightforward, they are rather hard to perform, as the above mentioned processes take place in microscopic (sub-millimetre) scales and the dimensions of the noise-reducing treatments are macroscopic. As a result, huge computational effort is needed for direct simulations. That is why sophisticated models have been developed, which introduce an effective fluid, see e.g. [1], which, in the macroscopic scale, mimics the behaviour of the structurally complicated porous media. These models employ sets of parameters, which can be calculated based on the micro-structural geometry of the porous material, see e.g. [2, 3, 4, 5, 6], which is somewhat an easier task than the direct numerical simulation, at least from the computational-effort point of view. In [7] the sound absorption of rigid porous media made up of identical rigid spheres in the face centered cubic packing (with porosity 26%) was calculated from micro-structure through its transport parameters and using the Johnson-Champoux-Allard-Pride-Lafarge (JCAPL) model [1, 8, 9, 10, 11, 12]. A similar approach for a similar problem of sound

propagation in granular media of rigid spheres, but in a few regular packings was investigated in [5] and [6]. Boutin and Geindreau [13] used the homogenization of periodic media to derive three estimates and also exact bounds of dynamic permeability in granular media of spherical grains. The micro-structure-based approach for modelling of porous media was also applied by Perrot et al. [3, 14] for open-cell aluminium foams and more recently for polymeric foams [15]. It was also applied for open foams with spherical pores in [16]. Chevillotte et al. [17] studied a link between microstructure and acoustical macro-behaviour of double porosity foams, and in [18] the microstructure-based approach was applied for 3D representations of fibrous materials.

As the computational power of contemporary computers incessantly increases, it becomes possible to perform the direct numerical simulations of the processes taking place in porous media even by employing desktop computers. Within the present work, the absorption of a plane wave impinging normally upon a rigid-wall-backed layer of spheres is studied by means of direct numerical simulations. The numerical results are compared with the ones obtained using the JCAPL model.

2. Mathematical model

2.1. Direct numerical simulation

As acoustic waves within the fluid filling the porous media frame propagate in narrow regions, viscous and thermal effects cannot be neglected and instead of a wave equation, linearised Navier-Stokes equations must be employed, see e.g. [1]. They can be written in form

$$\frac{\partial \rho'}{\partial t} + \rho_0 \boldsymbol{\nabla} \cdot \boldsymbol{v}' = 0, \tag{1a}$$

$$\rho_0 \frac{\partial \boldsymbol{v}'}{\partial t} - \boldsymbol{\nabla} \cdot \Big\{ -p' \boldsymbol{I} + \mu \Big[\boldsymbol{\nabla} \boldsymbol{v}' + (\boldsymbol{\nabla} \boldsymbol{v}')^{\mathrm{T}} \Big] - \frac{2\mu}{3} (\boldsymbol{\nabla} \cdot \boldsymbol{v}') \boldsymbol{I} \Big\} = \boldsymbol{0}, \tag{1b}$$

$$\rho_0 c_\mathrm{p} \frac{\partial T'}{\partial t} - \frac{\partial p'}{\partial t} - \kappa \boldsymbol{\nabla}^2 T' = 0, \tag{1c}$$

where ρ' is the acoustic density, $\boldsymbol{v}'$ is the acoustic velocity vector, p' is the acoustic pressure, ρ_0 is the fluid ambient density, μ is the shear viscosity, c_p is the specific heat at constant pressure, κ is coefficient of heat conduction and $\boldsymbol{I}$ is the identity matrix.

The set of equations (1) is supplemented with the linearised state equation of an ideal gas

$$\frac{p'}{p_0} = \frac{\rho'}{\rho_0} + \frac{T'}{T_0}, \tag{2}$$

where p_0 and T_0 are ambient pressure and temperature, respectively.

Within this work, it is assumed that the frame of the porous material is perfectly rigid (motionless) and the specific heat capacity of its material is much higher than the one of the fluid. As a result of that, Eqs. (1) are solved with no-slip and isothermal boundary conditions on the rigid surfaces

$$\boldsymbol{v}' = \boldsymbol{0}, \qquad T' = 0.$$

2.2. Equivalent fluid model

Under the long-wavelength approximation, when the characteristic microscale-structure dimensions are much smaller then the wavelength, the fluid in the complicated porous-media micro-scale geometry can be, in the macroscopic scale, replaced by an equivalent fluid with corresponding effective, frequency-dependent, and complex-valued properties; namely, the effective fluid density $\rho_\mathrm{c}(\omega)$ and effective fluid bulk modulus $K_\mathrm{c}(\omega)$. With these parameters, complex-valued characteristic impedance Z_c and the complex-valued wavenumber k_c can be introduced as

$$Z_\mathrm{c}(\omega) = \sqrt{\rho_\mathrm{c}(\omega) K_\mathrm{c}(\omega)}, \quad k_\mathrm{c} = \omega \sqrt{\frac{\rho_\mathrm{c}(\omega)}{K_\mathrm{c}(\omega)}}, \tag{3}$$

where ω is the angular frequency.

Once the porous-media micro-scale complexity has been homogenized-out, acoustic field in the porous media, instead of set of Eqs. (1) in the micro-scale, can be in the macroscopic scale calculated employing Helmholtz equation

$$\boldsymbol{\nabla} \cdot \left(\frac{1}{\rho_\mathrm{c}} \boldsymbol{\nabla} p' \right) + k_\mathrm{c}^2 p' = 0, \tag{4}$$

According to the JCAPL model [1, 16, 19], the effective properties can be written as

$$\frac{\rho_\mathrm{c}(\omega)}{\rho_0} = \frac{\nu \phi}{\mathrm{j}\omega k_0} \left[1 - b + b \sqrt{1 + \frac{\mathrm{j}\omega}{\nu} \left(\frac{2\alpha_\infty k_0}{b \phi \Lambda} \right)^2} \right] + \alpha_\infty, \tag{5}$$

where $\nu = \mu/\rho_0$ is the kinematic viscosity, ϕ is the porosity, k_0 is the viscous permeability, α_∞ is the tortuosity (at the frequency of ∞ Hz), Λ is the viscous characteristic length,

$$b = \frac{2 k_0 \alpha_\infty^2}{\phi \Lambda^2 (\alpha_0 - \alpha_\infty)},$$

where α_0 is the tortuosity (at the frequency of 0 Hz).

Further,

$$K_\mathrm{c}(\omega) = \frac{p_0}{1 - (\gamma - 1)/\gamma \alpha'(\omega)}, \tag{6}$$

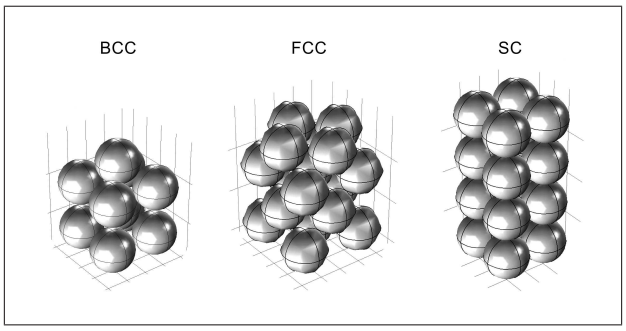

Figure 1. Sphere packing: body centered cubic (BCC), face centered cubic (FCC), and simple cubic (SC).

where p_0 is the ambient pressure, γ is the ratio of specific heats, and

$$\alpha'(\omega) = \frac{\nu'\phi}{\mathrm{j}\omega k_0'}\left[1 - b' + b'\sqrt{1 + \frac{\mathrm{j}\omega}{\nu'}\left(\frac{2k_0'}{b'\phi\Lambda'}\right)^2}\right] + 1, \quad (7)$$

where $\nu' = \nu/\mathrm{Pr}$, where Pr is the Prandtl number, k_0' is the thermal permeability, Λ' is the thermal characteristic length, and

$$b' = \frac{2k_0'}{\phi\Lambda'^2(\alpha_0' - 1)},$$

where α_0' is the thermal tortuosity (at the frequency of 0 Hz).

The eight parameters of the JCAPL model: ϕ, α_∞, α_0, α_0', k_0, k_0', Λ, and Λ' depend on the 'microscopic' structure of the rigid frame and in the case of a periodic rigid frame, they can be calculated numerically, solving the Stokes problem (steady-state incompressible flow), Laplace problem, and Poisson problem, see e.g. [5, 6], employing so-called representative volume element of the porous media. As the corresponding calculations are performed only on a representative cell of the porous media, they are numerically less expensive than the direct numerical simulations.

3. Numerical procedure

As an example, absorption of a plane wave impinging normally upon a rigid-wall-backed layer of rigid spheres is studied. Three periodic close packing configurations are assumed here: body centered cubic (BCC), face centered cubic (FCC), and simple cubic (SC), one, see Fig. 1.

3.1. Direct numerical simulations

The geometry of the computational domain for the direct numerical simulations is schematically shown in Fig. 2a. Thermoacoustics Interface of COMSOL

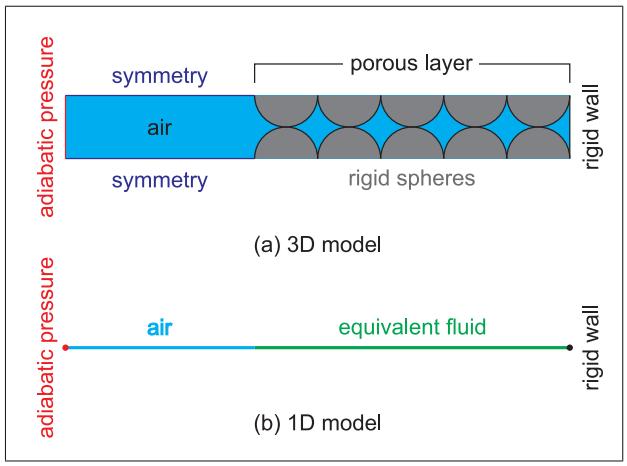

Figure 2. Schematics of the computational domain for DNS and the equivalent fluid model.

Multiphysics' Acoustics Module, see [19], is employed to solve Eqs. (1) numerically in the frequency domain. In all the studied cases, the smallest volume which repeats itself periodically is identified in order to minimize the necessary computational resources. The computational-domain periodicity is represented by symmetric boundary conditions (in all the studied cases, the ratio of the spheres' radii and the wavelength is so small that the impinging acoustic wave is not diffracted), impinging acoustic wave is represented by adiabatic-pressure boundary condition in some distance from the spheres. All the fluid–rigid-frame contact surfaces are treated by no-slip and isothermal boundary conditions.

Once the acoustic field within the computational domain is calculated, specific acoustic impedance at a point M, sufficiently far from the rigid spheres, is determined as

$$Z(M) = \frac{\tilde{p}'(M)}{\tilde{v}'(M)}, \quad (8)$$

where $\tilde{p}'$ represents the phasor of the acoustic pressure and $\tilde{v}'$ is the phasor of the acoustic velocity component along the direction of the wave propagation. With this information, the reflection coefficient modulus is calculated as

$$|\mathcal{R}| = \left|\frac{Z(M) - \rho_0 c_0}{Z(M) + \rho_0 c_0}\right|, \quad (9)$$

where c_0 is the speed of sound. As the porous layer is backed by a rigid wall (no wave transmission behind the layer), the absorption coefficient is calculated as

$$\alpha = 1 - |\mathcal{R}|^2. \quad (10)$$

Table I. Parameters for JCAPL model.

Parameter	Unit	SC	FCC	BCC
ϕ	%	47.80	26.18	32.19
ϕ (theor.)	%	47.80	26.17	32.19
α_∞	-	1.382	1.610	1.467
α_0	-	2.161	2.637	2.213
α_0'	-	1.418	1.851	1.345
k_0	$10^{-9}\,\mathrm{m}^2$	2.545	0.1781	0.5104
k_0'	$10^{-9}\,\mathrm{m}^2$	6.309	0.7035	1.015
Λ	$10^{-4}\,\mathrm{m}$	1.636	0.6395	0.9832
Λ'	$10^{-4}\,\mathrm{m}$	3.049	1.181	1.581
Λ' (theor.)	$10^{-4}\,\mathrm{m}$	3.049	1.181	1.581

3.2. Equivalent fluid model

As normal incidence is studied here, the model of equivalent fluid is a one-dimensional one, see Fig. 2b. The porous layer is represented by a layer of an equivalent fluid with thickness L. It can be easily shown that for the individual sphere packing, the layer thickness is

$$\begin{aligned} L_{\mathrm{SC}} &= 2Nr, \\ L_{\mathrm{BCC}} &= \frac{2}{\sqrt{3}}(N+1)r, \\ L_{\mathrm{FCC}} &= \left[2+\sqrt{2}(N-1)\right] r, \end{aligned} \tag{11}$$

where $N > 1$ is the number of the spheres across the layer, and r is the spheres' radius.

The effective parameters ρ_c, K_c are calculated employing formulas (5) and (6). The eight parameters of the JCAPL model are calculated in COMSOL Multiphysics following the procedure described in [5, 6]. The porous surface specific acoustic impedance is calculated by formula, see e.g. [1]

$$Z_\mathrm{s} = -\mathrm{j} Z_\mathrm{c} \cot(k_\mathrm{c} L), \tag{12}$$

where Z_c and k_c are given in Eq. (3). From here, the absorption coefficient is calculated using Eqs. (9) and (10), the impedance $Z(M)$ is replaced by Z_s though.

4. Numerical results

As the fluid, air at normal conditions was assumed, the distance between the neighbouring 'touching' spheres was set to $s = 1\,\mathrm{mm}$ and the spheres' radius (for the computational convenience) as $r = 0.999\,s/2$.

The parameters for the JCAPL model are given in Tab. I together with corresponding analytical values of the porosity and thermal characteristic length, which can be calculated easily using analytical formulas, see [1, 5, 6]. The mesh-convergence study and the comparison with the analytical results indicates that the parameters should be determined with the accuracy of at least three significant digits.

Figures 3–5 show the comparison of the frequency characteristics of the absorption coefficient of sphere layers with different thicknesses and the sphere packing, as calculated employing direct numerical simulation (markers) and the JCAPL model (lines). In the figures, N represents the number of the spheres across the layer. It can be seen that both the computational approaches provide very similar results, even though there are some discrepancies, especially in the case of

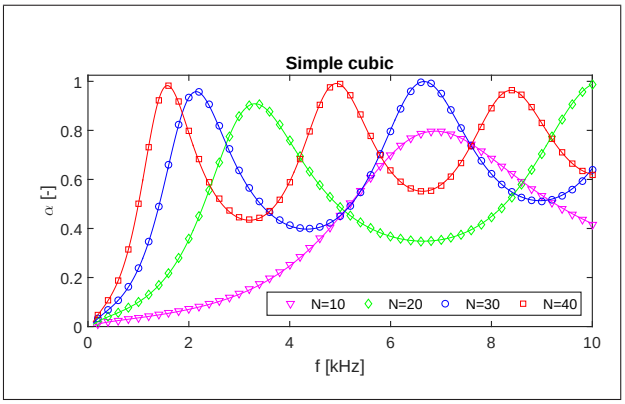

Figure 3. Absorption coefficient of a layer of N spheres; simple cubic packing; N is the number of spheres across the layer; DNS (markers), JCAPL model (lines).

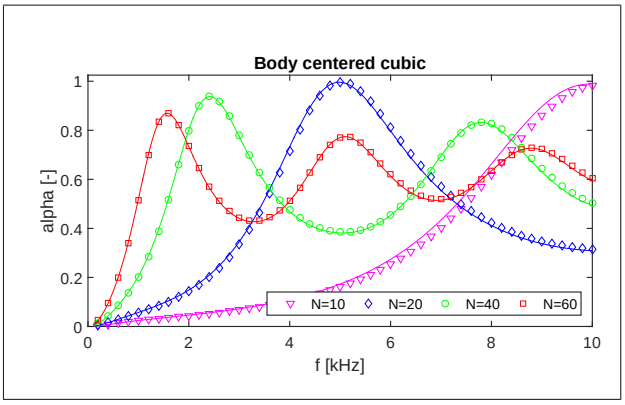

Figure 4. Absorption coefficient of a layer of N spheres; body centered cubic packing; N is the number of spheres across the layer; DNS (markers), JCAPL model (lines).

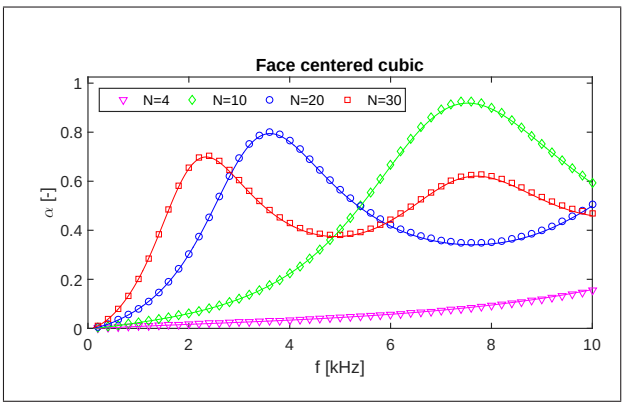

Figure 5. Absorption coefficient of a layer of N spheres; face centered cubic packing; N is the number of spheres across the layer; DNS (markers), JCAPL model (lines).

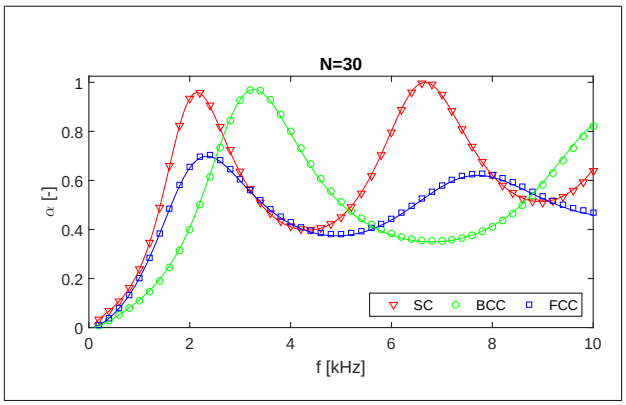

Figure 6. Absorption coefficient of layers with $N = 30$ spheres across the layer and individual sphere packings; DNS (markers), JCAPL model (lines).

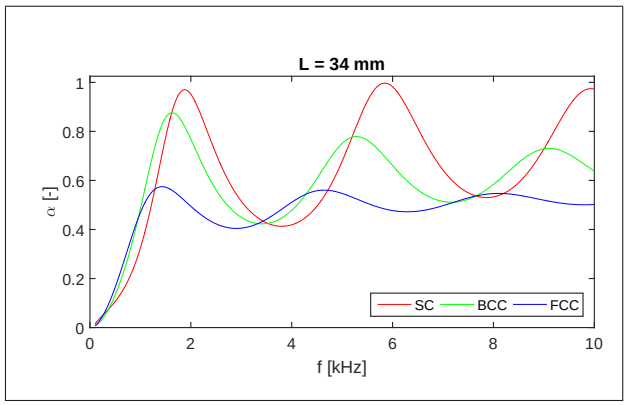

Figure 7. Absorption coefficient for layers with different sphere packing, but approximately the same width $L \approx 34$ mm; calculated employing JCAPL model; SC: $N = 34$, BCC: $N = 58$, FCC: $N = 48$.

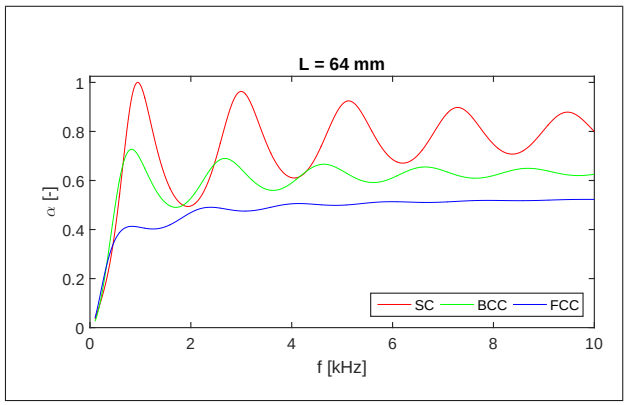

Figure 8. Absorption coefficient for layers with different sphere packing, but approximately the same width $L \approx 64$ mm; calculated employing JCAPL model; SC: $N = 64$, BCC: $N = 110$, FCC: $N = 90$.

the BCC packing and $N = 10$, see Fig. 4. Subsequent refinement of the mesh has shown that this discrepancy is not caused by a numerical error; moreover, the situation improves with the number of the spheres N in the layer, as it can be expected.

In order to obtain this good agreement (Figs. 3 – 5), we had to use the maximum finite-element size of 1/10 of the cubic cell size and 5 mesh-boundary-layers within the viscous boundary layer thickness along the no-slip surfaces. The boundary layer thickness was calculated and the computational mesh was re-generated for each of the frequencies of interest. Most of the calculations were performed on a desktop computer with 128 GB of RAM, it was observed that the amount of allocated memory increased with frequency.

Figure 6 shows the comparison of the absorption properties of layers with individual packaging types; in all the cases, the number of spheres across the layer is the same, $N = 30$. It can be observed that the frequency of the first absorption peak differs for individual packing types, which is partly caused by the fact that for given N, the layer widths are different (in this case, $L_{\mathrm{SC}} = 30\,\mathrm{mm}$, $L_{\mathrm{BCC}} = 17.9\,\mathrm{mm}$, and $L_{\mathrm{FCC}} = 21.5\,\mathrm{mm}$). It can also be seen, that the difference between the absorption coefficient peaks and troughs are much bigger for the SCC and BCC packings than for the FCC packing – the former two ones have 'more resonant' character.

Figures 7–8 show the comparison of the absorption coefficient for individual types of sphere packing, however, in this case, the layer widths are approximately the same (there are different number of spheres N across the layer).

In Fig. 7, SC: $N = 34$, $L_{\mathrm{SC}} = 34\,\mathrm{mm}$, BCC: $N = 58$, $L_{\mathrm{BCC}} = 34.06\,\mathrm{mm}$, FCC: $N = 48$, $L_{\mathrm{FCC}} = 34.23\,\mathrm{mm}$. In Fig. 8, SC: $N = 64$, $L_{\mathrm{SC}} = 64\,\mathrm{mm}$, BCC: $N = 110$, $L_{\mathrm{BCC}} = 64.08\,\mathrm{mm}$, FCC: $N = 90$, $L_{\mathrm{FCC}} = 63.93\,\mathrm{mm}$. It can be observed in the figures that as the layers for individual sphere packings have the same width, the first resonance can be found at approximately the same frequency. The absorption characteristics for the SC packing has the most prominent resonant character of all the sphere packings. For bigger layer widths, it can be said that the SC packing outperforms the BCC and FCC one with the smallest number of spheres across the given layer width.

5. Conclusions

Within this work, it has been shown that 3D DNS of poroacoustic processes can be performed on contemporary personal computers if the corresponding geometry allows reducing the volume of the computational domain. As an example, absorption characteristics of differently-packed sphere-layers were studied. The obtained numerical results are mesh-converged, and a very good agreement with the results provided by equivalent-fluid-model (JCAPL) has been found. Even if the 3D DNS are much slower than the calculations employing models of equivalent fluid, they offer the possibility to study e.g. the configurations with stratified properties. Nevertheless, it should be men-

tioned, that from the computational point of view, it is much easier to study the configurations/cases where the ratio of the characteristic micro-structure geometrical details dimensions and the viscous boundary layer thickness is not too big.

Acknowledgement

This research collaboration is supported by COST (European Cooperation in Science and Technology) through the COST Action CA15125 – *DENORMS: "Designs for Noise Reducing Materials and Structures"*. M. Červenka and M. Bednařik were financially supported by GACR grant GA18-24954S and by The Ministry of Education, Youth and Sports from the Large Infrastructures for Research, Experimental Development and Innovations project "IT4Innovations National Supercomputing Center – LM2015070". T.G. Zieliński would like to acknowledge the financial support of the Project "*Relations between the micro-geometry and sound propagation and absorption in porous and poroelastic media*", No. 2015/19/B/ST8/03979, financed by the Polish National Science Centre (NCN).

References

[1] J.-F. Allard, N. Atalla: Propagation of Sound in Porous Media: Modelling Sound Absorbing Materials, Second Edition, Wiley, 2009.

[2] A. M. Chapman, J. J. L. Higdon: Oscillatory Stokes flow in periodic porous media. Phys. Fluids A 4 (1992) 2099–2116.

[3] C. Perrot, R. Panneton, and X. Olny: Periodic unit cell reconstruction of porous media: Application to open-cell aluminum foams. J. Appl. Phys. 101 (2007) 113538.

[4] C. Perrot, F. Chevillotte, and R. Panneton: Bottom-up approach for microstructure optimization of sound absorbing materials. J. Acoust. Soc. Am. 124 (2008), 940–948.

[5] Ch.-Y. Lee, M. J. Leamy, J. H. Nadler: Acoustic absorption calculation in irreducible porous media: A unified computational approach. J. Acoust. Soc. Am. 126 (2009) 1862–1870.

[6] T. G. Zieliński: Microstructure-based calculations and experimental results for sound absorbing porous layers of randomly packed rigid spherical beads. J. Appl. Phys. 116 (2014) 034905.

[7] S. Gasser, F. Paun, and Y. Bréchet: Absorptive properties of rigid porous media: Application to face centered cubic sphere packing. J. Acoust. Soc. Am. 117 (2005), 2090–2099.

[8] D. L. Johnson, J. Koplik, and R. Dashen: Theory of dynamic permeability and tortuosity in fluid-saturated porous media. J. Fluid Mech. 176 (1987) 379–402.

[9] Y. Champoux and J.-F. Allard: Dynamic tortuosity and bulk modulus in air-saturated porous media. J. Appl. Phys. 70 (1991) 1975–1979.

[10] S. R. Pride, A. F. Gangi, and F. D. Morgan: Deriving the equations of motion for porous isotropic media. J. Acoust. Soc. Am. 92 (1992) 32780–3290.

[11] S. R. Pride, F. D. Morgan, and A. F. Gangi: Drag forces of porous medium acoustics. Phys. Rev. B 47 (1993) 4964–4978.

[12] D. Lafarge, P. Lemarinier, J. F. Allard, and V. Tarnow: Dynamic compressibility of air in porous structures at audible frequencies. J. Acoust. Soc. Am. 102 (1997) 1995–2006.

[13] C. Boutin, and C. Geindreau. Periodic homogenization and consistent estimates of transport parameters through sphere and polyhedron packings in the whole porosity range. Phys. Rev. E: Stat., Nonlinear, Soft Matter Phys. 82 (2010) 036313.

[14] C. Perrot, F. Chevillotte, and R. Panneton: Dynamic viscous permeability of an open-cell aluminum foam: Computations versus experiments. J. Appl. Phys. 103 (2008) 024909.

[15] C. Perrot, F. Chevillotte, M. T. Hoang, G. Bonnet, F.-X. Bécot, L. Gautron, and A. Duval: Microstructure, transport, and acoustic properties of open-cell foam samples. Experiments and three-dimensional numerical simulations. J. Appl. Phys. 111 (2012) 014911.

[16] T. G. Zieliński: Generation of random microstructures and prediction of sound velocity and absorption for open foams with spherical pores. J. Acoust. Soc. Am. 137 (2015) 1790–1801.

[17] F. Chevillotte, C. Perrot, and E. Guillon: A direct link between microstructure and acoustical macrobehavior of real double porosity foams. J. Acoust. Soc. Am. 134 (2013), 4681–4690.

[18] T. G. Zieliński: Microstructure representations for sound absorbing fibrous media: 3D and 2D multiscale modelling and experiments. J. Sound Vib. 409 (2017) 112–130.

[19] COMSOL Multiphysics – Acoustics Module User's Guide, COMSOL, 2017.